Bulletin of Earthquake Engineering (2020) 18:1499–1524
https://doi.org/10.1007/s10518-019-00755-5

ORIGINAL RESEARCH

Experimental seismic response evaluation of suspended piping restraint installations

Daniele Perrone[1] · **Andre Filiatrault**[1,2] · **Simone Peloso**[3] · **Emanuele Brunesi**[3] · **Clemens Beiter**[4] · **Roberto Piccinin**[4]

Received: 17 April 2019 / Accepted: 19 November 2019 / Published online: 23 November 2019

Abstract
Observations from recent earthquakes have repeatedly demonstrated that damage to non-structural elements can significantly compromise the capacity of critical facilities to continue services during times of crises. Performance-based seismic design requires the harmonization of performances between structural and non-structural elements. Among the multitude of non-structural typologies, the seismic performance of piping systems is of paramount importance in order to guarantee the immediate post-event functionality of critical facilities. Few research studies are available in the literature that provide information on the seismic response of piping systems, and in particular of suspended piping restraint installations. This paper presents and discusses the results of an experimental program designed to evaluate the seismic behavior of suspended piping restraint installations. Four typologies of suspended piping restraint installations were tested under monotonic and reversed cyclic loading to determine their hysteretic responses and failure modes and to evaluate key response parameters.

Keywords Suspended piping restrains · Non-structural elements · Piping systems · Cyclic testing

1 Introduction

The seismic design of non-structural elements is nowadays recognized to be a key issue in the performance-based seismic design of new buildings and the retrofit of existing ones. The influence of non-structural elements in the performance-based seismic design as well as in the seismic loss estimation framework is mainly related to two issues: (1)

✉ Daniele Perrone
daniele.perrone@iusspavia.it

1 University School for Advanced Studies IUSS Pavia, Pavia, Italy

2 Department of Civil, Structural, and Environmental Engineering, State University of New York at Buffalo, Buffalo, USA

3 European Centre for Training and Research in Earthquake Engineering, Pavia, Italy

4 Hilti Corporation, Schaan, Liechtenstein

non-structural elements generally exhibit damage at low seismic intensities with respect to supporting structures and (2) non-structural elements represent most of the total investments in typical buildings (Miranda and Taghavi 2003). The more recent advanced (FEMA 2018) and simplified (FEMA 2003; Kia et al. 2018, 2019) methodologies available in the literature to perform loss estimation studies account for the influence of non-structural elements. Loss estimation studies performed on existing buildings demonstrated that the loss related to non-structural elements are generally higher with respect to the losses associated to structural elements, in particular for low seismic intensities (O'Reilly et al. 2018; Sousa and Monteiro 2018).

The post-earthquake functionality of critical facilities, such as hospitals, relies on the continued operation of non-structural elements including piping systems, partitions, ceiling systems and other medical equipment. The damage suffered by non-structural elements, particularly piping systems, during recent earthquakes demonstrated their vulnerability and importance for the immediate serviceability of buildings (Miranda et al. 2012; Fleming 1998; Perrone et al. 2018). Following the 2010 Chile earthquake, for example, the Santiago International Airport was closed for several days because of the severe damage to piping systems interacting with ceiling systems (Miranda et al. 2012). During the same earthquake, four hospitals completely lost their functionality and over 10 lost almost 75% of their functionality due to damage to sprinkler piping systems (Miranda et al. 2012). During the 1994 Northridge earthquake in California, the leakage and water damage resulting from piping system failures forced the temporary evacuation of some buildings (OSHPD 1995). Similar inadequate performance of piping systems was also observed following the 2006 Hawaii Earthquake (Chock et al. 2006). The poor seismic performance of piping systems, and in particular of pressurized suppression sprinkler piping systems, were generally due to the inadequate bracing of the pipes. Inadequately or improperly restrained piping systems may suffer damage as a result of large differential displacements of the system or from the impact with adjacent structural and non-structural elements.

Although poor seismic performance of non-structural elements has been observed repeatedly in past earthquakes, very limited research results are available to better understand the seismic behaviour of these components, and specifically of piping systems. The seismic performance of piping systems depends on the piping material and the joint typology as well as on the bracing system installed. The piping systems are typically supported from floor or roof slabs by hanger-rods or trapezes designed for gravity loads. In seismic regions, the pipes need to be restrained laterally and longitudinally at discrete locations along their length by seismic (sway) braces (Malhotra et al. 2003). Despite the availability of empirical guidelines to provide recommendations for the installation of seismic bracing in piping systems (NFPA13 2019; FEMA E-74 2012), extensive systematic experimental data is not available to understand the real response of piping joints and restraint installations under reverse cyclic loading. The seismic performance of piping joints was studied recently by Tian et al. (2014a, b) during an extensive experimental program. Tian et al. (2014a) tested 48 pressurized tee joint specimens made of various diameters and made of different materials and connection types through monotonic and reverse cyclic loading to determine their rotational capacity at first leakage. The same authors also tested four different full scale pressurized sprinkler piping subsystems with various levels of seismic bracing under dynamic loading (Tian et al. 2014b). Hoehler et al. (2009) studied also the performance of suspended pipes installed in a seven storeys reinforced concrete building tested on a large shake table. The study was mainly devoted to evaluate the performance of the anchorages used to connect the trapeze systems to the rigid floor. Zaghi et al. (2012) studied the seismic response of hospital piping assemblies with and without seismic restraints subjected to various intensities of seismic loading. The hysteretic response of piping braces was analysed by Malhora et al. (2003) who tested also two pipe-attached components and two building-attached components. Based on their results, the authors proposed a uniform-amplitude deformation-controlled loading protocol to measure the seismic strength of brace components. Finally, Wood et al. (2014) reported on the seismic response of two typologies of suspended trapeze assemblies made of metal struts through monotonic and reversed cyclic displacement control tests. The results demonstrated that the load-displacement behaviour of trapeze assemblies is mainly affected by the joints connecting the trapeze elements.

To properly understand the seismic performance of non-structural elements, an extensive experimental database is still required (Perrone and Filiatrault 2017). Suspended trapeze assemblies are commonly installed in industrial and commercial facilities including offices, hospitals, stores, and civil infrastructure to support various services systems, such as piping and cable trays. Many typologies of suspended trapeze ceiling installations are available. The most common ones are the channel frame and the rod trapeze installations, as shown in Fig. 1. These trapezes consist of multiple channel (or rod) elements connected through specialized connections. The displacement and acceleration demand transmitted by the supporting trapeze systems onto the pipes and connected equipment items could significantly affect the serviceability of buildings in the aftermath of an earthquake.

This paper contributes to the development of the experimental database on the seismic performance of piping restraint installations by presenting and discussing the results of an experimental program carried out to evaluate the seismic performance of four common typologies of suspended trapeze installations. The suspended piping restraint installations and supported pipes were tested under monotonic and reverse cyclic loading to determinate their load-displacement hysteretic responses as well as their failure modes. The results were analysed in term of global response parameters and damage states.

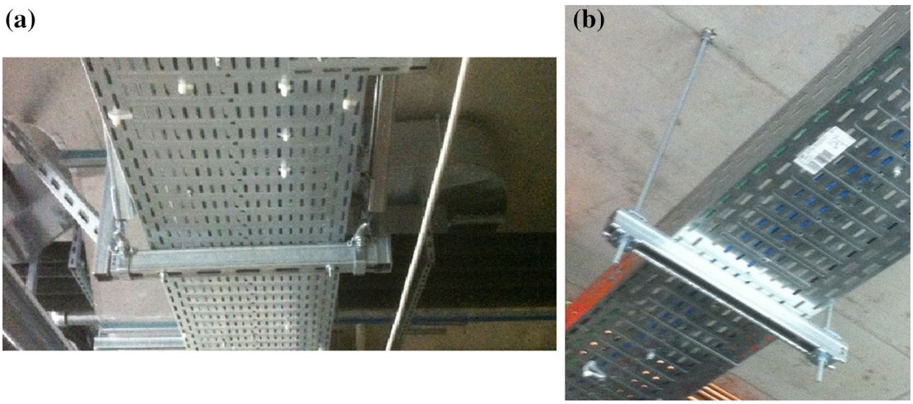

Fig. 1 Typical examples of trapeze assemblies: **a** Channel frame installation, **b** Rod trapeze installation

2 Description of suspended trapeze test assemblies

The seismic restraint of suspended non-structural elements (i.e. piping systems) can be achieved through many typologies of sway bracing systems or trapeze installations. A field survey was carried out to identify most common typologies of trapeze assemblies installed in industrial and commercial buildings in Europe, with a special focus on Italy. The seismic installation systems are divided into two main categories: ceiling applications and wall applications. Most used installation supports are ceiling applications made of channel frames or rod trapezes. Based on this information, the four ceiling applications shown in Fig. 2 were selected for testing.

The first typology consists of a trapeze with transverse channel bracing (Fig. 2a), referred herein as “SS1”. This configuration typically includes four steel channels with section dimensions depending on the application and the applied load. Generally, the channel depth can range from 21 to 120 mm and in this study the more common channel size equal to 41 mm square was retained. The distance from the ceiling to the horizontal channel is 800 mm, while the length of the horizontal channel is also 800 mm. The diagonal channel is inclined at an angle of 45° from the vertical. Similar considerations in terms of channel size and length apply to the trapeze braced in the longitudinal direction, referred to in this study as “SS2” (Fig. 2b). Also in this case, the typical distance from the ceiling to the horizontal channel is equal to 800 mm. The third typology considered consists of trapeze assemblies with transversal rod bracing (Fig. 2c). This third “SS3” configuration includes four threaded rods with a diameter of 10 mm. The distance between the ceiling and the horizontal channel is assumed equal to 600 mm, while the length of the horizontal channel

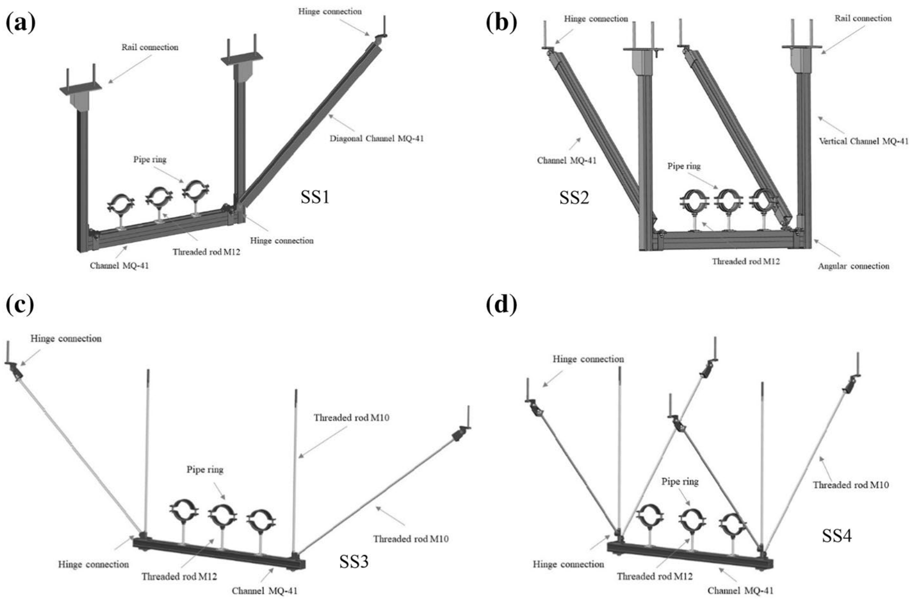

Fig. 2 Suspended trapeze test assemblies: **a** Trapeze with transverse channel bracing system (SS1), **b** Trapeze with longitudinal channel bracing system (SS2), **c** Trapeze with transverse rod bracing system (SS3), **d** Trapeze with longitudinal rod bracing system (SS4)

is equal to 900 mm. The last "SS4" typology consists of an installation with longitudinal rod bracing (Fig. 2d). Also in this case, the distance from the ceiling to the horizontal channel is equal to 600 mm, while the length of the horizontal channel is equal to 900 mm. Six threaded rods with a diameter equal to 10 mm are mounted and are inclined by an angle of 45° from the vertical. The connections between the steel channels and the diagonal threaded rods elements are guaranteed by hinges and rail supports. In particular, for the SS1 and SS2 configurations, the vertical channels are connected to the horizontal channel by angles and each diagonal channel is connected to the ends of the horizontal channel and to the ceiling slab by channel hinges. For the SS3 and SS4 typologies, the vertical and diagonal threaded rods are connected to the horizontal channels by seismic hinges. Finally, for all four typologies, all vertical and diagonal members are connected to the top floor slab by rail supports. Table 1 summarizes the main geometrical characteristics of the suspended trapeze test assemblies.

3 Description of experimental set-up

The experimental set-up to conduct the monotonic and reverse cyclic tests on the selected suspended piping restraint installations consisted of a 3 m high steel frame (Fig. 3a) connected to the strong floor of the laboratory through a system of steel beams and post-tensioned bars.

The frame was designed to have stiffness at least two order of magnitude greater than the stiffest specimen, hence assuring negligible deformation and elastic energy accumulation during the tests. The design resulted in two coupled HE140A sections for each column, HE140A beam girder supporting the top plates and two UPN200 acting as diagonal braces. Finite element analyses of the frame confirmed that the chosen configuration satisfied the requirements. The steel frame supported three 1.5 m × 3.5 m × 15 mm thick horizontal steel plates. The system of steel plates, which served as the support for the specimens, could be shifted upward or downward (by means of steel corbels that can be fixed along the steel columns at different heights) to adapt the setup configuration to the different heights of the specimens, avoiding to move the horizontal actuator along the vertical direction. The system of steel plates had two sets of holes: the first one was used to connect the plates to the H-shaped beam girder and to the columns; the second set of holes was necessary to install the specimens. All the connections were bolted.

A reaction wall supported the horizontal actuator that applied load to the test specimens suspended and connected to the plates of the steel frame. The influence of the anchors was not taken into account in the experimental program because previous tests demonstrated that, when properly designed and installed, anchors did not affect the response of suspended piping restraints (Hoehler et al. 2009). Two trapeze installations were loaded

Table 1 Main geometrical properties of suspended trapeze test assemblies

ID	Frame typology	Bracing direction	Brace inclination (°)	Number of braces	Length (mm)	Heigth (mm)
SS1	Channel	Transverse	45°	1	800	800
SS2	Channel	Longitudinal	45°	2	800	800
SS3	Rod	Transverse	45°	2	900	600
SS4	Rod	Longitudinal	45°	4	900	600

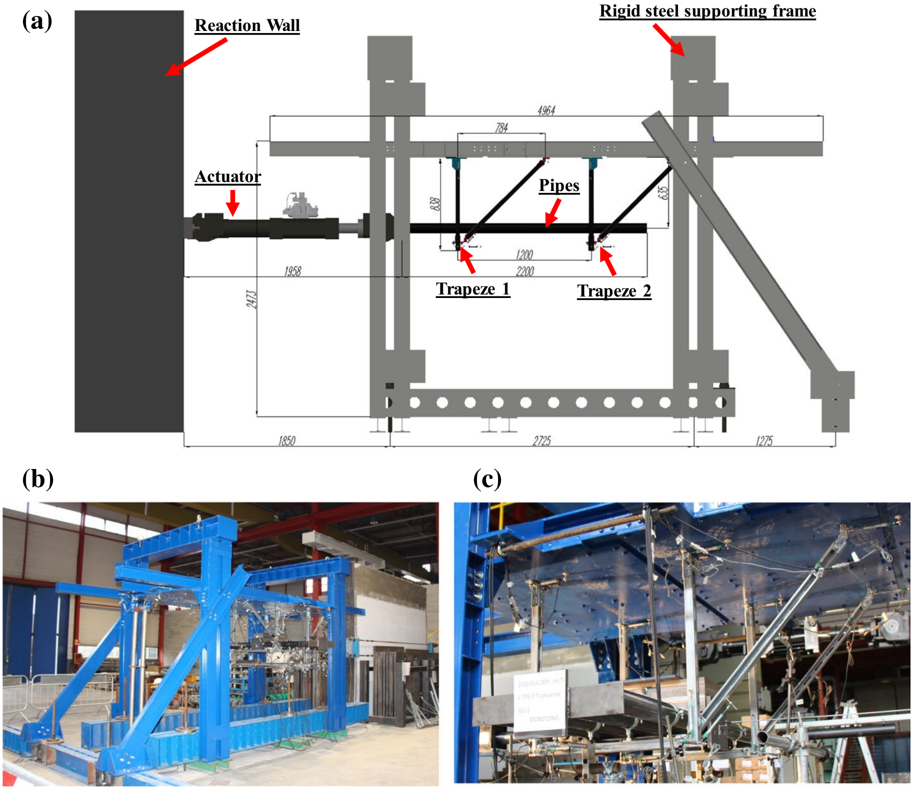

Fig. 3 **a** Lateral view of the experimental set-up; **b** Photograph of experimental set-up. and **c** Close-up of SS2 test specimen

simultaneously during each test. The number of anchors used to connect each trapeze installation to the steel plates depended on the trapeze configurations: for the SS1 configuration, five anchors were necessary, for the SS2 and SS4 configurations six anchors were used, while for the SS3 configuration four anchors connected the trapeze to the supporting structure. As described in Sect. 2, the tested trapezes were selected after a field survey carried out to identify the most used suspended piping restraint installations in Italy. All the components used to assembly the trapeze installations were not specifically designed for this experimental study but were taken from the typical configurations available on the market. The distance between the two trapeze installations was equal to one meter *to accommodate the available laboratory space*. The suspended piping restraint installations were designed for gravity loads. The gravity load on the trapeze installations was simulated by a tributary weight applied by four rigid steel pipes connected to the trapeze installations and an additional mass located at mid-span of the pipes. A gravity weight of 1.5 kN was applied in each test to simulate a typical configuration of four steel pipes supported by adjacent trapeze installations spaced 3 m apart (Hilti 2014). Figure 3c shows a close-up photograph of the SS2 configuration under test (in this case the load is applied in the perpendicular to the direction of the pipe axis). In order to simulate the application of inertia forces to the test specimens, the load from the horizontal actuator was applied directly to

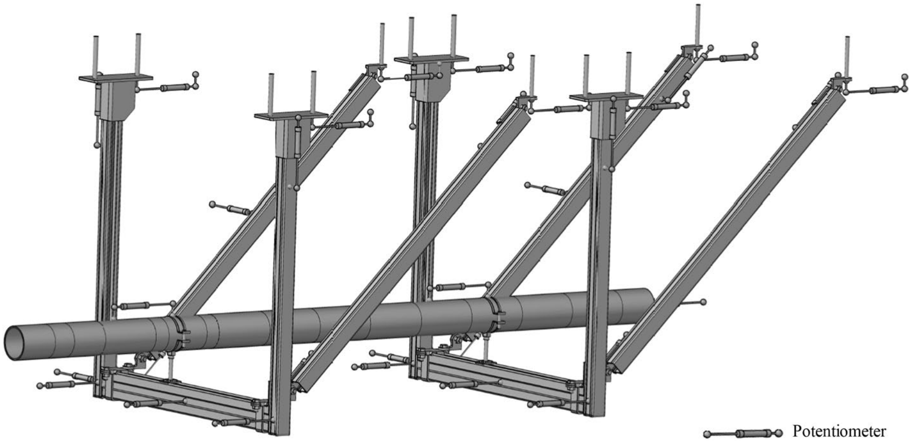

Fig. 4 Potentiometers locations for SS2 test specimen (only one of four pipes shown for clarity)

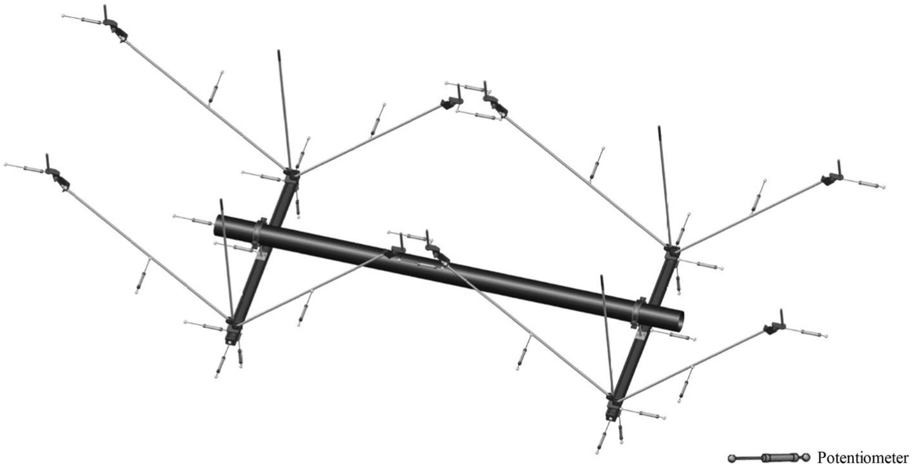

Fig. 5 Potentiometers Locations for SS4 test specimen (only one of four pipes shown for clarity)

the pipes that were attached to the trapeze installations by means of stiff pipe rings and short threaded rods with a diameter equal to 12 mm. The use of short threaded rods and stiff pipe rings insured that they did not control the ultimate capacity of the test assemblies.

An array of potentiometers was used to measure displacements at key locations on the test specimens. The forces in the threaded rods were measured by installing miniature load cells in series with the threaded rods. The locations of the potentiometers are shown in Figs. 4 and 5 for configurations SS2 and SS4, respectively. To make the figures clearer only one of the four horizontal pipes is shown. A similar array of potentiometers was also used to measure the displacements for configurations SS1 and SS3. All the displacements of the base connections were measured as well as the relative displacements between the connections of the vertical, horizontal and diagonal elements. The possible out-of-plane deformation as well as the sliding between the pipes and the pipe rings, were also measured. Eight potentiometers were installed at the base of the steel frame in order to verify that no movement or deformation of the reaction frame occurred during the tests. The displacements applied to the test specimens were also monitored by a temposonic position sensor connected to the opposite side and offset of the actuator. The comparison between the displacement recorded by the temposonic sensor and the actuator allowed to better capture the rotation of the specimen.

Table 2 lists all the details of the 12 tests that were carried out during the experimental program. All specimens were tested in their braced directions. For each configuration, one monotonic and two cyclic tests were performed. The monotonic tests were used to calibrate the corresponding cyclic loading protocol, as described in Sect. 4.

4 Loading protocol

Two types of tests were carried out on each of the selected suspended trapeze configurations. First, a monotonic test was performed (Table 2). The monotonic loading protocol consisted of a linear ramp until the maximum actuator displacement limit or the failure of the subsystem occurred. Failure of a test specimen was defined when a 20% decay of the maximum horizontal load was observed. A slow loading rate was set equal to 0.5 mm/s for each monotonic test in order to avoid inertia effects.

The cyclic tests were carried out following the FEMA 461 quasi-static cyclic loading protocol (FEMA 2007). The FEMA 461 loading protocol is considered the most appropriate loading protocol available in the literature to perform cyclic tests on non-structural elements in order to evaluate response parameters and observe the damage propagation (Filiatrault et al. 2018). The loading history consists of repeated cycles of step-wise increasing deformation amplitudes, in particular two cycles at each amplitude were considered. Table 3 lists all the parameters required to reproduce the quasi-static cyclic loading protocol used for each configuration. In this table, Δ_o is the target smallest deformation amplitude of the loading history and Δ_m represents the target maximum deformation amplitude of the loading history obtained from a preliminary monotonic test. The number of amplitudes required to reach Δ_m is also listed in Table 3.

Table 2 Description of experimental program

Test ID	Configuration cyclic test	Brace direction	Load direction	Monotonic test	Cyclic tect
1	SS1	Transversal	Transversal	X	
2	SS1	Transversal	Transversal		X
3	SS1	Transversal	Transversal		X
4	SS2	Longitudinal	Longitudinal	X	
5	SS2	Longitudinal	Longitudinal		X
6	SS2	Longitudinal	Longitudinal		X
7	SS3	Transversal	Transversal	X	
8	SS3	Transversal	Transversal		X
9	SS3	Transversal	Transversal		X
10	SS4	Longitudinal	Longitudinal	X	
11	SS4	Longitudinal	Longitudinal		X
12	SS4	Longitudinal	Longitudinal		X

Table 3 Details of cyclic loading protocol for each sub-assembly configuration

Configuration	Load direction	D_o (mm)	Target D_m (mm)	Number of amplitudes
SS1	Transversal	1.0	21.3	10
SS2	Longitudinal	1.7	36.0	10
SS3	Transversal	1.3	27.0	10
SS4	Longitudinal	4.5	91.9	10

5 Experimental results

In this section, the main results of the experimental campaign are discussed in terms of observed damage and load-displacement relationships. The results for both monotonic and cyclic tests are provided and compared in terms of backbone curves.

5.1 Test results for configuration SS1

5.1.1 Monotonic test results

The first monotonic test was conducted on a configuration SS1 specimen in the transverse direction of the supported pipes. The load-displacement response measured during this first monotonic test is shown in Fig. 6. The recorded maximum load was equal to 14.1 kN, corresponding to a displacement of the actuator equal to 19 mm. Due to the yielding of the channel hinge connecting the brace channel and the vertical channel in one of the two trapezes, the applied load decreased to 10 kN (29% degradation of peak force) at a displacement of 21 mm (Fig. 7a). This yielding of the channel hinge caused differential translations between the two trapezes and a significant rotation of the specimen, as shown in Fig. 7b. For the remaining of the test, the adjacent trapeze continued to attract load causing an increase of the load from 10 kN, to approximately 13 kN at the end of the monotonic test, corresponding to a final displacement of 100 mm.

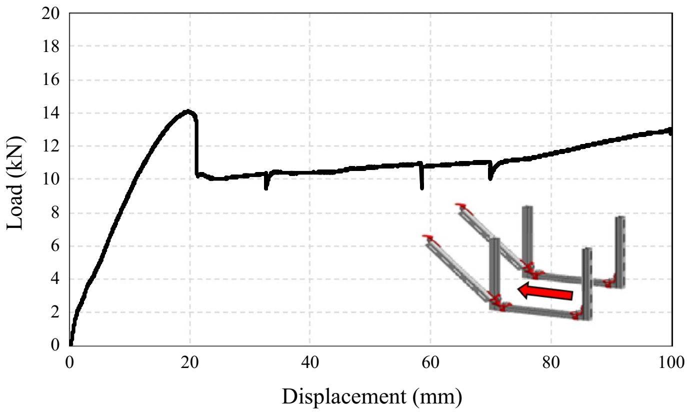

Fig. 6 Experimental monotonic load-displacement response from configuration SS1

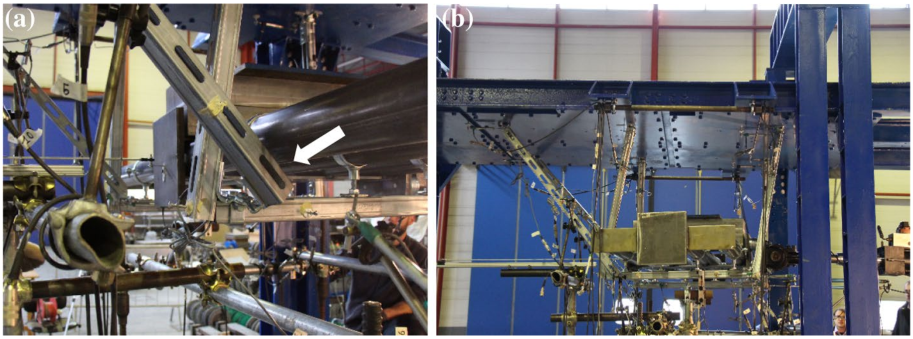

Fig. 7 Damage observed during monotonic test on configuration SS1: **a** Yielding of the channel hinge connecting the diagonal brace and the vertical channel in one of the two trapezes, **b** Displaced shape of specimen at maximum displacement

5.1.2 Cyclic test results

Two SS1 specimens were subjected to reverse cyclic displacements along the transversal pipe direction according to the cyclic loading protocol described in Sect. 4. Figure 8 shows the hysteretic load-displacement responses recorded during these two tests, along with the monotonic load-displacement response. The maximum compressive and tensile loads are equal to 16.1 kN and 18.9 kN, respectively for the first cyclic test. The corresponding maximum compressive and tensile loads are 12.9 kN and 19.0 kN, respectively for the second cyclic test. The maximum displacements achieved during the first test are equal to 63 mm in compression and 78 mm in tension. The corresponding displacement values are 53 mm in compression and 61 mm in tension for the second test. The overall hysteretic responses of the two specimens are similar, both in terms of hysteretic shapes and damage observation. The first drop in compression strength was due to the yielding of one of the channel hinges connecting the brace to the vertical channel, as shown in Fig. 9a. The yielding of the channel hinge occurred at similar displacements in the two tests (20 mm and 16 mm). The second drop in compression strength observed in both tests at a displacement close to 40 mm was due to the disconnection of the diagonal brace from the horizontal channel as a consequence of the significant rotations of the specimens, as shown in Fig. 9b. Each test

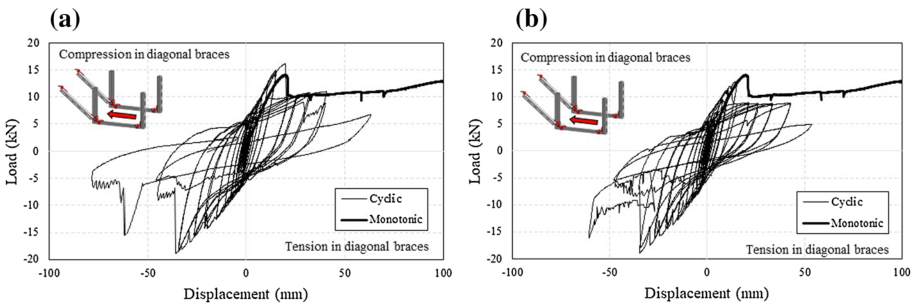

Fig. 8 Experimental hysteretic load-displacement responses from configuration SS1: **a** First specimen and **b** Second specimen

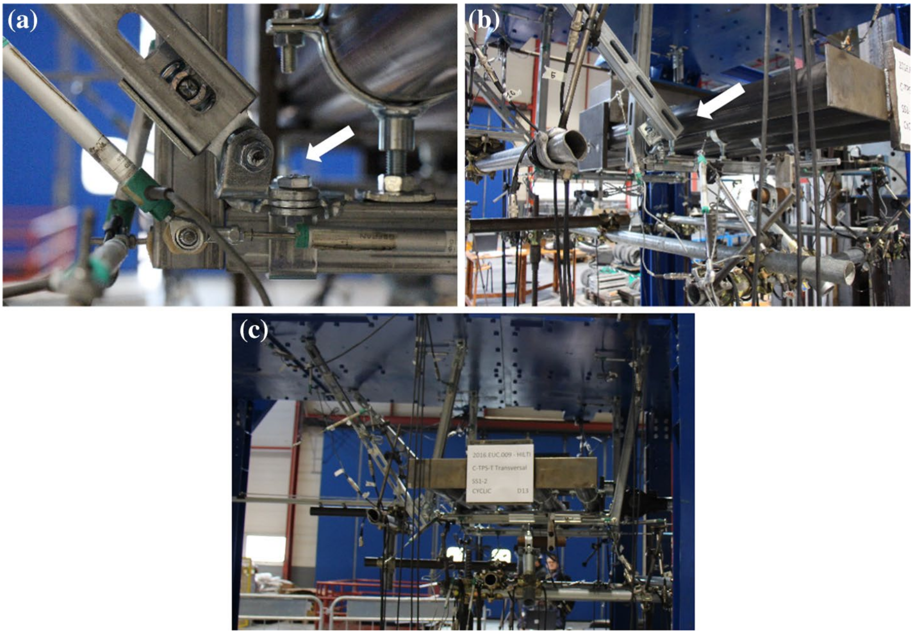

Fig. 9 Damage observed during cyclic tests on configuration SS1: **a** Yielding of the channel hinge connecting the diagonal brace and the vertical channel, **b** Disconnection of the diagonal brace (at a displacement of approximately of 40 mm), **c** Displaced shape of first specimen at maximum displacement

was stopped when the second diagonal brace disconnected from the horizontal channel, as shown in Fig. 9c. Note that at the end of both tests, the gravity load carrying capacities of the specimens were not compromised by the induced damage. In general, a good match is observed between the monotonic and cyclic responses, both in terms of stiffness and maximum load, as also reported in Table 4.

Table 4 Response parameters obtained from monotonic and cyclic tests on suspended piping restraints

Test ID	Configuration	Test protocol	Qm (kN)	K_I (kN/mm)	$\Delta_{Y,eff}$ (mm)	Δ_U (mm)	μ_{eff}	E_{af} (kNmm)	ξ_{eq} (%)
1	SS1	Monotonic	14.1	1.0	14.3	21.1	1.5	–	–
2	SS1	Cyclic	17.4	1.4	13.1	28.4	2.2	939.8	18
3	SS1	Cyclic	15.8	1.4	12.0	25.1	2.1	622.4	18
4	SS2	Monotonic	19.1	1.0	19.1	38.9	2.0	–	–
5	SS2	Cyclic	23.4	1.6	17.0	60.7	3.6	1581.2	15
6	SS2	Cyclic	23.7	1.5	15.8	60.8	3.8	1703.0	16
7	SS3	Monotonic	12.5	2.7	4.6	21.2	4.6	–	–
8	SS3	Cyclic	13.4	2.5	5.6	24.1	4.3	670.6	12
9	SS3	Cyclic	10.9	1.8	6.2	13.4	2.2	511.0	11
10	SS4	Monotonic	22.2	1.3	17.2	50.0	2.9	–	–
11	SS4	Cyclic	21.4	1.6	13.5	69.6	5.1	1320.3	14
12	SS4	Cyclic	18.9	1.7	11.4	46.4	4.1	865.6	13

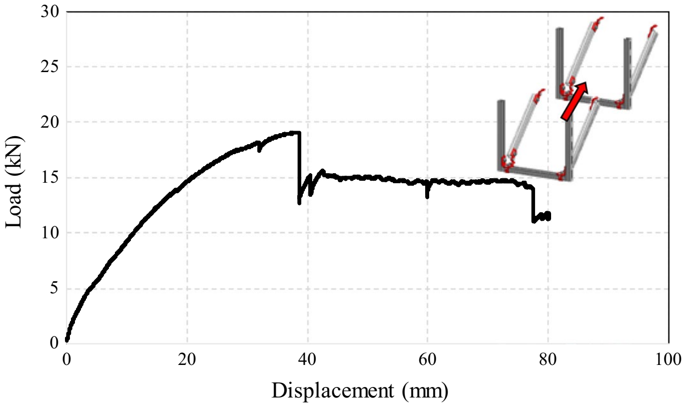

Fig. 10 Experimental monotonic load-displacement response from configuration SS2

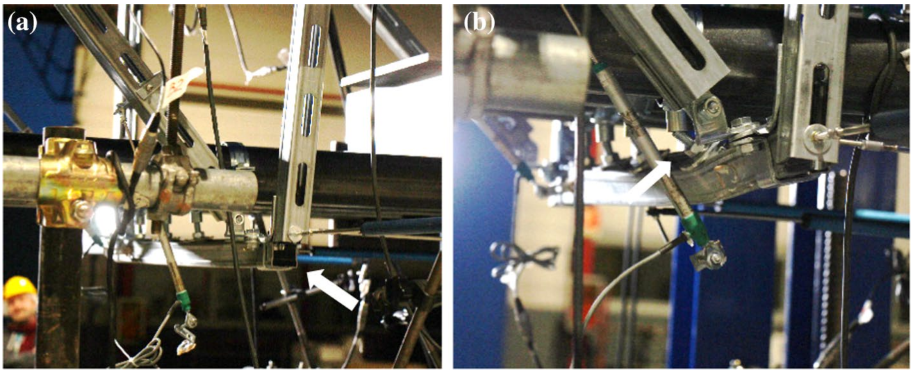

Fig. 11 Damage observed during monotonic test on configuration SS2: **a** Sliding of the connection between the vertical and horizontal channel, **b** Failure of a threaded rod connecting the pipe ring to the horizontal channel

5.2 Test results for configuration SS2

5.2.1 Monotonic test results

The second monotonic test was conducted on a configuration SS2 specimen in the longitudinal direction of the supported pipes. Figure 10 reports the monotonic load-displacement response obtained during the test. The recorded maximum load was equal to 19.1 kN corresponding to a displacement in the actuator equal to 39 mm. At a displacement equal to 40 mm, the threaded rods connecting the pipe-rings to the horizontal channel were substantially deformed. In one of the two trapeze specimens, torsional rotation of the horizontal channel was observed due to the high deformation of two of the four threaded rods connecting the pipe-rings to the horizontal channel. In the other trapeze specimen, the horizontal channel moved downwards due to the sliding of the component connecting the vertical and horizontal channels (Fig. 11a). Due to the different damage in the left and right trapezes, the rigid system of pipes supported by the specimens experienced a significant rotation. At a displacement level of 80 mm, the test was stopped due to the failure of a threaded rod connecting a pipe-ring to the horizontal channel in one of the trapezes (Fig. 11b). No further damage was observed in the base connections or in the braces until the end of the monotonic test.

5.2.2 Cyclic test results

Two SS2 specimens were subjected to reverse cyclic displacements along their longitudinal directions according to the cyclic loading protocol described in Sect. 4 and calibrated according to the monotonic test results described in Sect. 5.2.1. The hysteretic load-displacement responses measured during these two cyclic tests are shown in Fig. 12, along with the monotonic load-displacement response. The overall responses of the two specimens are very similar. In both cases, the maximum load in compression is approximately equal to 20.0 kN, while the load in tension is approximately equal to 27.0 kN, which represents a difference of 34% between compressive and tensile capacities. The maximum displacement achieved during the two tests is equal to 61 mm both in compression and tension.

Up to a displacement of 20 mm, no damage was observed in both specimens. Starting at a displacement equal to 36 mm, a significant rotation of the specimen around the vertical axis was observed along with an important deformation of the threaded rods connecting the pipe rings to the horizontal channels (Fig. 13a, b). During the last portions of the tests, differential vertical displacements between the two sides of the specimens were observed. Both cyclic tests concluded with the shear failure in one of the threaded rods connecting a pipe ring to the horizontal channel (Fig. 13c). Flexural and torsional yielding of the horizontal channel were also observed in both specimens (Fig. 13c). Although the initial stiffness observed in the monotonic response is slightly lower with respect to the initial stiffness observed during the cyclic tests, the overall responses of the monotonic and cyclic tests are similar.

5.3 Test results for configuration SS3

5.3.1 Monotonic test results

During the third monotonic test, a specimen SS3 was tested in the transverse direction of the supported pipes. For this specimen, special retainers were provided to the vertical

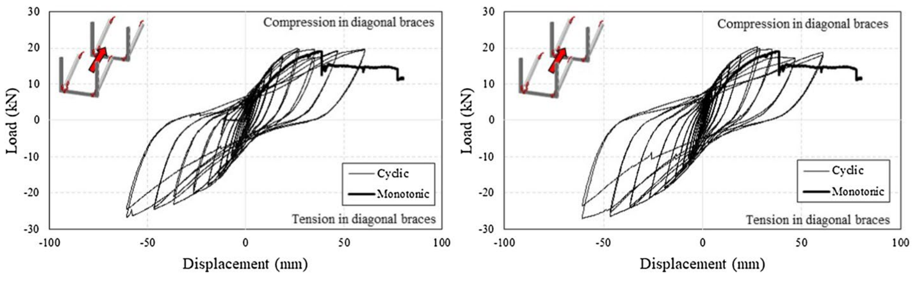

Fig. 12 Experimental hysteretic load-displacement responses from configuration SS2: **a** First specimen and **b** Second specimen

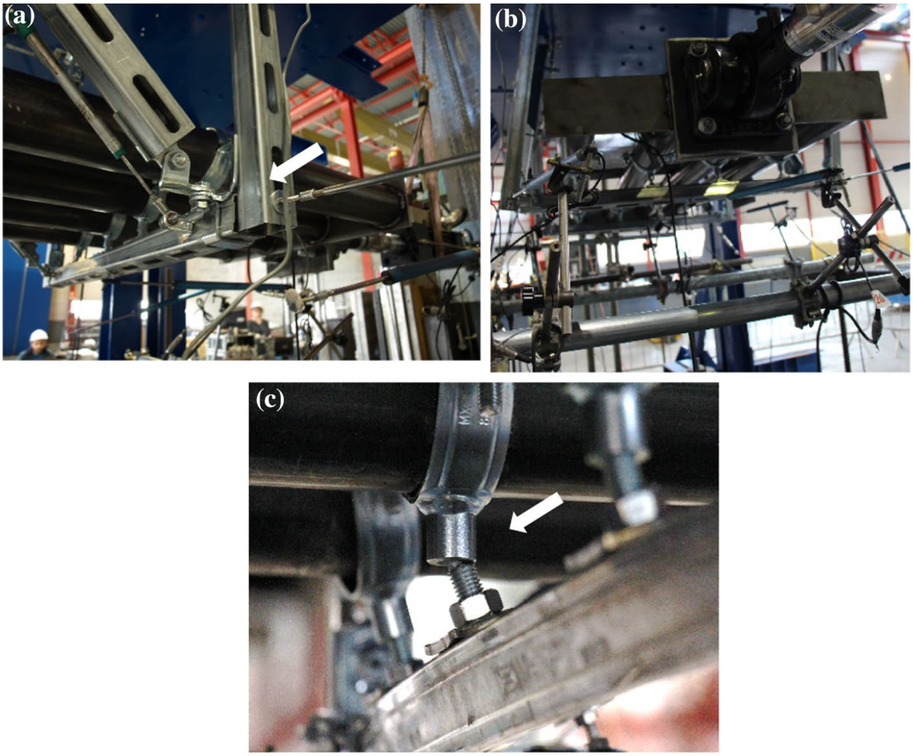

Fig. 13 Damage observed during cyclic tests on configuration SS2: **a** Deformation in the connection between vertical and horizontal channels, **b** Rotation of the specimen, **c** Failure of a threaded rod connecting a pipe-ring to the horizontal channel

rods in order to prevent them from buckling prematurely. These special retainers consist of channels within which the vertical threaded rods are constrained using special radial bolts. The load-displacement response obtained during this monotonic test is shown in Fig. 14.

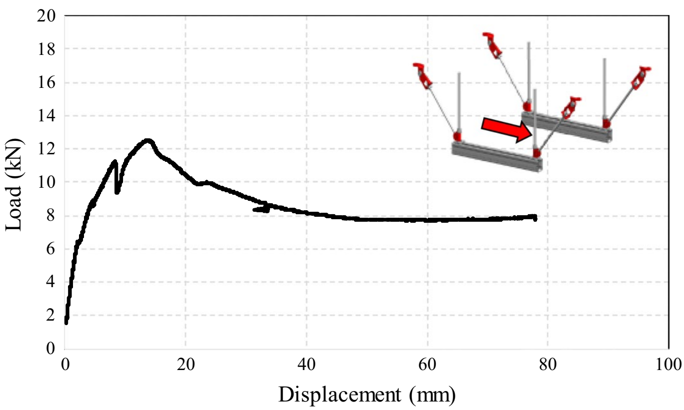

Fig. 14 Experimental monotonic load-displacement response from configuration SS3

The maximum load recorded during the test was equal to 12.5 kN, corresponding to a displacement of the actuator equal to 14 mm. The load dropped to 8 kN at the maximum displacement (more than 75 mm).

At a displacement of 40 mm, the braces buckled in compression. In one of the two trapezes, the brace exhibited an evident in plane deformation, while in the other trapeze the brace was subjected to an out-of-plane deformation (Fig. 15a). Due to the different deformation of the braces in the two trapezes, a global rotation of the specimen was observed. A significant out-of-plane deformation of the vertical rods was also observed. At a displacement equal to 78 mm, the test was stopped because of the large rotation of the actuator's swivel in the vertical plane. At this stage, the vertical rods as well as the braces in compression were permanently deformed. A rotation in the vertical plane was also observed due to the high deformation of the threaded rods in both trapezes (Fig. 15b). No failure of the components (e.g. local failure at the connections between the channel and the vertical rods) was observed during this monotonic test.

5.3.2 Cyclic test results

The same SS3 configuration tested in Sect. 5.3.1 was tested with the cyclic loading protocol described in Sect. 4. Two different SS3 specimens were tested. The vertical rods of the first specimen included retainers while the vertical rods of the second specimen were unrestrained.

The hysteretic load-displacement responses obtained during the two cyclic tests are plotted in Fig. 16, along with the monotonic load-displacement response. For the first specimen, the maximum load in compression was equal to 14.2 kN, while a maximum load equal to 12.7 kN was reached in tension. The maximum compressive and tensile loads reached in the second test were equal to 11.4 kN and 10.4 kN, respectively. The maximum displacement achieved during the two cyclic tests was equal to 76 mm both in compression and in tension.

At a displacement equal to 5 mm, the deformation of the diagonal rods became evident in both specimens. Due to the presence of the vertical retainers, the deformation of the vertical rods was different for the two specimens (Fig. 17a–c). The retainers significantly influenced the deformation of the vertical rods during the first cyclic test: a double curvature was observed in their deformed shape (Fig. 17a). The braces mainly

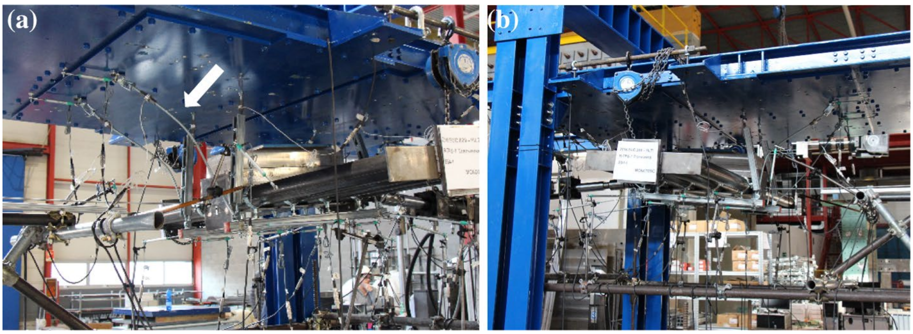

Fig. 15 Damage observed during monotonic test on configuration SS3: **a** Buckling in compression of the diagonal rods, **b** Deformed shape of the specimen at maximum displacement

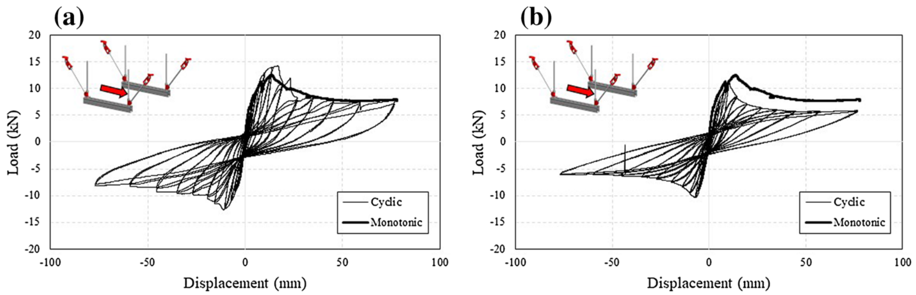

Fig. 16 Experimental hysteretic load-displacement responses from configuration SS3: **a** First specimen and **b** Second specimen

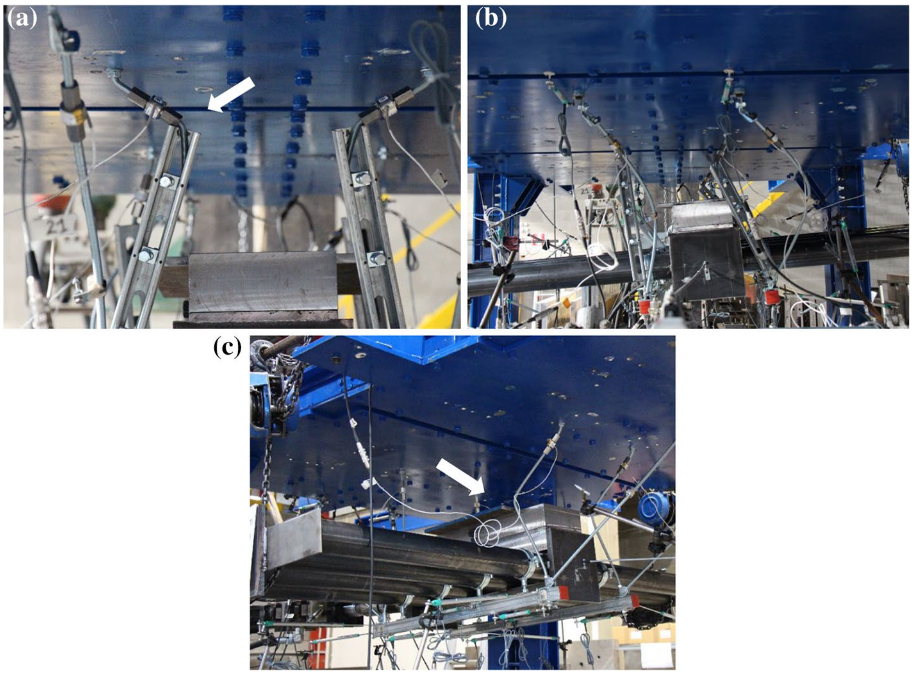

Fig. 17 Damage observed during cyclic tests on configuration SS3: **a** Deformation of the vertical rods restrained with channels in the first cyclic test, **b** Out-of-plane rotation of the specimen in the first cyclic test, **c** Deformation of the vertical rods and rotation of the specimen in the second cyclic test

deformed out of the plane of the specimen. The pipe-rings did not suffer any damage nor significant deformation during these cyclic tests. At a displacement equal to 76 mm, a significant rotation of the specimen both in plane and out of plane was observed in both cyclic tests (Fig. 17b). The two tests were stopped due to the large deformations of the trapezes and to the large rotation of the actuator in the horizontal and vertical plane. No component failures were reported at the end of the tests. A good match was

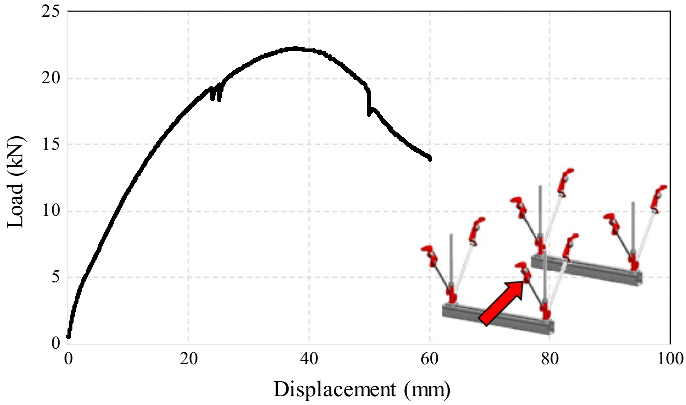

Fig. 18 Experimental monotonic load-displacement response from configuration SS4

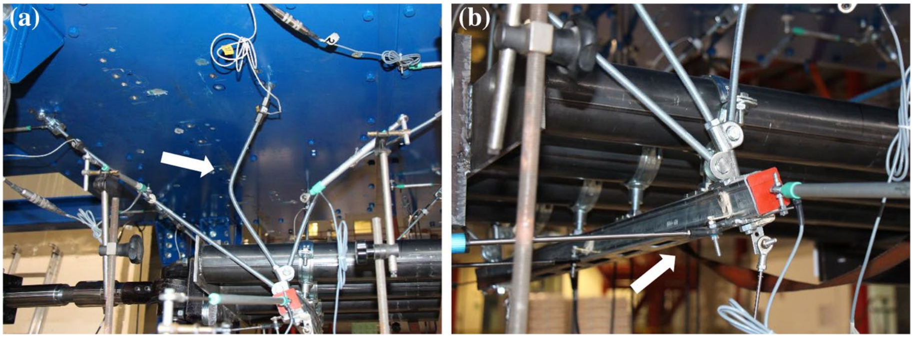

Fig. 19 Damage observed during monotonic test on configuration SS4: **a** Deformation of the vertical rods and bracing rods, **b** Torsion of the horizontal channel

observed between the monotonic and cyclic response, in particular in the specimen which included retainers in the vertical rods.

5.4 Test results for configuration SS4

5.4.1 Monotonic test results

The last monotonic test was conducted on a SS4 specimen in the longitudinal direction of the supported pipes. The monotonic load-displacement response recorded during the test is shown in Fig. 18. The maximum load is equal to 22.2 kN, corresponding to a displacement in the actuator of 37 mm. At a displacement of 25 mm, out of plane deformations of the diagonal rods were observed (along the direction perpendicular to the actuator). As the displacement increased further, the horizontal channels experienced both flexural and torsional yielding, as shown in Fig. 19b. This flexural-torsional yielding of the channels caused also inelastic deformations in the short threaded rods connecting the pipe-rings to the horizontal channels. The threaded rods of the inner pipe-rings deformed more than those of the outer pipe rings. As shown in Fig. 19a, at a displacement equal to 50 mm a significant deformation of the diagonal and vertical rods was observed. At this stage, the torsion of the horizontal channels increased with high inelastic torsional deformations near the ends of the channels. Due to the high level of deformation of the braces, particularly on one side of the specimen, the rotation about the vertical axis of the specimen was also observed. The test was stopped at a displacement equal to 60 mm because the applied load dropped beyond 20% of its maximum value. No component failure was observed at the end of the test.

5.4.2 Cyclic test results

The experimental program concluded by subjecting two SS4 specimens to reverse cyclic displacements along their longitudinal direction according to the cyclic loading protocol described in Sect. 4. The hysteretic load-displacement responses obtained during the tests are shown in Fig. 20, along with the monotonic load-displacement response. The maximum compressive and tensile loads are equal to 23.3 kN and 19.6 kN, respectively for the first cyclic test. The corresponding maximum compressive and tensile loads are 21.0 kN and 17.0 kN, respectively for the second specimen. The maximum displacement achieved during the tests was equal to 92 mm both in compression and in tension. At a displacement equal to 10 mm, a limited in-plane buckling of the diagonal rods took place in both specimens. A small rotation of the specimen about the vertical axis was also observed. Due to the opposite deformations of the diagonal rods, the rotation of the entire specimen around the pipes direction was observed (Fig. 21c). High torsional deformations of the horizontal channels, close to the connection with the vertical and diagonal rods, was also observed (Fig. 21b). At a displacement equal to 92 mm, all vertical and diagonal rods were significantly deformed (Fig. 21a). The deformation angle of two vertical rods approached 90°. Due to the reduction of the horizontal load carrying capacity as well as to the large deformations of the threaded rods, the tests were stopped. When the actuator was returned to its initial position, the deformations of the rods were only partially recovered. A very good match was observed between the monotonic and cyclic load-displacement responses, as also observed comparing the response parameters reported in Table 4.

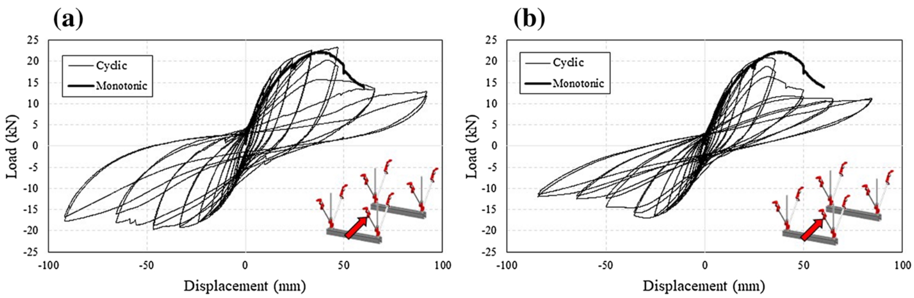

Fig. 20 Experimental hysteretic load-displacement responses from configuration SS4: **a** First specimen and **b** Second specimen

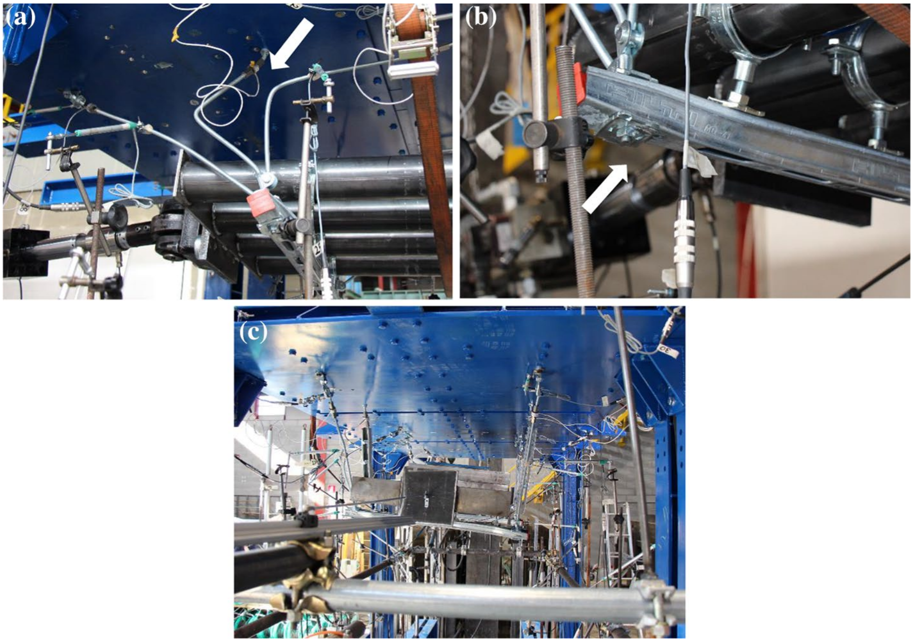

Fig. 21 Damage observed during cyclic tests on configuration SS4: **a** Deformation of the vertical rods, **b** Torsion of the horizontal channel, **c** Global rotation of the specimen

6 Evaluation of response parameters

Based on the FEMA P-795 (FEMA 2011) methodology for structural elements, some simple response parameters can be defined based on the results of the monotonic and cyclic tests conducted on the suspended piping restraints discussed in the previous section. The following seven response parameters were identified from the hysteretic load-displacement responses of the suspended piping restraint installations tested.

1. Maximum load (Q_M): maximum load capacity;
2. Initial stiffness (K_I): initial stiffness based on force and deformation at 0.4 Q_M;
3. Effective yield displacement (Δ_Y): defined as the ratio Q_M/K_I;
4. Ultimate deformation (Δ_U): deformation corresponding at $0.8Q_M$ in the post peak range;
5. Effective ductility (μ_{eff}): defined as the ratio Δ_U/Δ_Y;
6. Total absorbed energy (E_{af}): area under the cyclic envelope at the final amplitude of the cyclic tests;
7. Mean equivalent viscous damping ratio (ξ_{eq}): mean value of damping ratio taken across all cycles according to the Jacobsen's equal area formulation (Jacobsen 1960).

The first five response parameters are illustrated in Fig. 22.

Table 4 lists the response parameters evaluated for each tested configuration. The mean values between the positive and the negative envelopes are reported for the cyclic tests. The maximum loads (Q_M) are obtained for the configurations braced in the longitudinal direction, this is the consequence of the higher number of braces installed

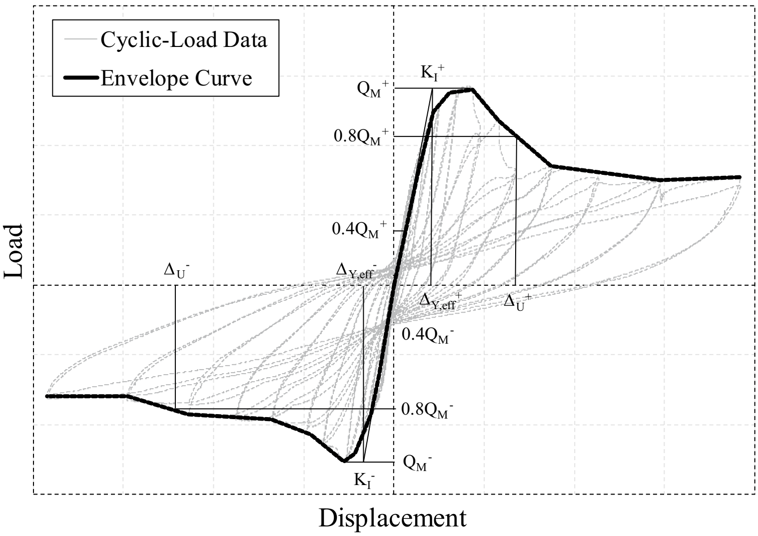

Fig. 22 Definition of response parameters [after FEMA (2011)]

in these configurations (respectively two and four for configuration SS2 and SS4). The initial stiffness is comparable between the different configurations, with the highest stiffness obtained for configuration SS3. In terms of ductility, the rod suspended piping restraints show higher ductility than that of the channel frame configurations. This behaviour is mainly related to the lower displacement at which yielding first occurred in the rod trapeze installations. The highest equivalent viscous damping ratio was obtained for channel suspended piping restraint installations tested in the transverse direction ($\xi_{eq} = 18\%$), while in the longitudinal direction ξ_{eq} is approximately equal to 15%. For rod configurations, $\xi_{eq} = 11\%$ and 13% in the transverse and longitudinal direction, respectively. For similar brace arrangements and direction, higher strength capacity and energy dissipation is observed in the channel frame configurations, while higher ductility is obtained in the rod trapezes installations due mainly to lower yield displacements.

7 Correlation between performance objectives and Engineering Demand Parameters

The application of the Performance-Based Earthquake Engineering framework for the seismic design/assessment of non-structural elements requires the definition of some parameters, referred as Engineering Demand Parameters (EDPs), which allows to correlate the achievement of a performance objective to the damage experienced by the non-structural elements (Krawinkler 1999; Yang et al. 2009; Filiatrault and Sullivan 2014). Different performance objectives can be defined for non-structural elements based on the seismic intensity and on the limit states established by building codes. In most building codes (CEN 2004; ASCE 2016), the following two general non-structural performance objectives are stated:

- Damage limitation performance objective (DL): Non-structural elements may show minor damage, but the damage could be economically repaired and does not affect the functionality of the building (e.g. minor yielding or elastic buckling in some components of piping restraint installations). The DL performance objective corresponds to frequent earthquakes with a typical probability of exceedance of the order of 50% in 50 years;
- Life safety performance objective (LS): Non-structural elements can be damaged, but without compromising life-safety (e.g. piping system restraint braces are damaged but trapezes still holding the pipes). The LS performance objective corresponds to design earthquakes with a typical probability of exceedance of 10% in 50 years;

The non-structural performance objectives stated above can be applied to suspended piping restraint installations. Depending on the approach followed by designers, each of the response parameters described in Sect. 6 could be assumed as EDP for the design of suspended piping restraint installations. However, the most simple and suitable approach could be to express the EDP in terms of displacement or ductility. The DL performance objective, for which the functionality of the building is not affected, can be associated with the effective yield displacement ($\Delta_{Y,eff}$ in Table 4) or, alternatively, with an effective ductility factor (μ_{eff} in Table 4) equal to unity. Maintaining elastic response allows to minimize the economic losses as well as to guarantee the immediate functionality of the piping systems supported by the suspended trapezes. The LS performance objective can be associated with the ultimate deformation (Δ_U) in Table 4 or, alternatively, with the effective ductility factor (μ_{eff}) shown in Table 4. For lateral displacements smaller than Δ_U, suspended piping restraint installations are still able to carry the gravity loads, which will both ensure life-safety and safe evacuation of the building by the occupants. Table 5 lists the effective ductility factor (μ_{eff}) associated with each damage performance objective for the four suspended piping restraints configurations tested. The values of μ_{eff} listed in Table 5 correspond to the mean values obtained from the monotonic and two cyclic tests conducted on each configuration (see Table 4).

The results of the monotonic and cyclic tests can now be used to evaluate the effectiveness of the effective ductility factor (μ_{eff}) as the performance parameter for suspended piping restraints. This can be achieved by recording the displacements during each test for which the first occurrence of damage corresponding to the DL and LS damage objectives occurred.

Tables 6, 7, 8, 9 report, for each tested suspended piping restraint configuration, the effective experimental ductility ratios ($\mu_{eff,exp}$) for which the onset of damage corresponding to each performance objective occurred. A description and photographs of each damage observation are also provided. Each value of $\mu_{eff,exp}$ reported in Tables 6, 7, 8, 9 represents the ratio between the displacement at the onset of the relevant damage

Table 5 Effective ductility factors associated with performance objectives of suspended piping restraints

Performance objective	Effective ductility factor, μ_{eff}			
	SS1 configuration	SS2 configuration	SS3 configuration	SS4 configuration
DL	1.0	1.0	1.0	1.0
LS	1.9	3.1	3.7	4.0

Table 6 Correlation between EDPs, onset of damage and performance objectives for configuration SS1

Configuration	Performance objective	EDP $\mu_{eff,exp}$	Damage description	Photographs
SS1	DL	Monotonic Test = 1.5 Cyclic Test 1 = 1.5 Cyclic Test 2 = 1.3 **Mean = 1.4**	Yielding of the channel hinge connecting the brace channel and the vertical channel in one of the two trapezes	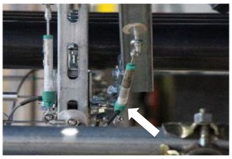
	LS	Monotonic Test = 7.0 Cyclic Test 1 = 6.0 Cyclic Test 2 = 5.1 **Mean = 6.0**	Significant rotation of the specimen around the vertical axis Disconnection of the diagonal braces from the horizontal channels Sliding between one diagonal brace and the hinge connection with the rigid floor (only in Test 2) The gravity load carrying capacity of the specimen was not compromised by the induced damage	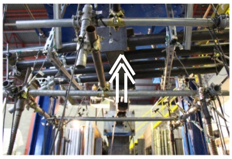 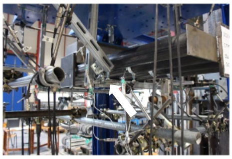

divided by the corresponding effective yield displacements listed in Table 4. Because the gravity load carrying capacity of the suspended piping restraint installations was never compromised during any of the tests, the maximum displacement achieved in each test was used to compute $\mu_{eff,exp}$ associated with the LS performance objective. All effective experimental ductility ratios ($\mu_{eff,exp}$) reported in Tables 6, 7, 8, 9 are larger than the effective ductility factors (μ_{eff}) listed in Table 5. This result indicates that the effective ductility factor (μ_{eff}) is an adequate and conservative EDP for predicting performance.

8 Conclusions

The results of monotonic and reverse cyclic tests on 12 suspended piping restraint installations were described in this paper. The main objective of this study was to determine suitable response parameters and engineering demands parameters (EDPs) for predicting performance objectives of suspended piping restraint installations. A field survey was first carried out to identify the most common typologies of sway bracing systems in commercial, industrial and strategical buildings. Based on the results of the field survey, the following four typologies of suspended piping restraint installations were tested: (1) trapezes with transverse channel bracing systems, (2) trapezes with longitudinal channel bracing systems, (3) trapezes with transverse rod bracing systems and, (4) trapezes with longitudinal rod bracing systems. For each installation, three tests were conducted: one monotonic and two cyclic tests according to the FEMA

Table 7 Correlation between EDPs, onset of damage and performance objectives for configuration SS2

Configuration	Performance Objective	EDP $\mu_{eff,exp}$	Damage Description	Photographs
SS2	DL	Monotonic Test = 1.7 Cyclic Test 1 = 1.5 Cyclic Test 2 = 1.6 **Mean = 1.6**	Deformation of the threaded rods connecting the pipe-rings to the horizontal channel Torsional and bending deformation of the horizontal channel due to the high deformation of two of the four threaded rods The horizontal channel moved downwards due to the sliding of the component connecting the vertical and horizontal channels (occurred in Monotonic Test only)	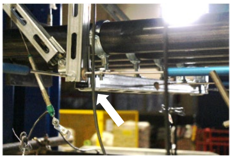
	LS	Monotonic Test = 4.2 Cyclic Test 1 = 3.6 Cyclic Test 2 = 3.9 **Mean = 3.9**	Failure of a threaded rod connecting a pipe-ring to the horizontal channel in one of the two trapezes (occurred in Monotonic and Cyclic test 2) Significant rotation of the specimen around the vertical axis The horizontal channel moved downwards due to the sliding of the component connecting the vertical and horizontal channels (occurred in Monotonic Test only) The gravity load carrying capacity of the specimen was not compromised by the induced damage	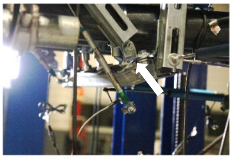 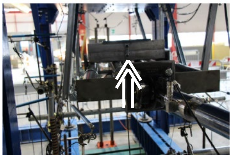

461 loading protocol. From the results of the tests, the following main conclusions can be drawn:

- All suspended piping restraints exhibited a significant strength capacity varying from 14.1 to 23.7 kN for the channel trapezes and from 12.5 to 22.2 kN for the rod configurations.

Table 8 Correlation between EDPs, onset of damage and performance objectives for configuration SS3

Configu-ration	Performance objective	EDP $\mu_{eff,exp}$	Damage description	Photographs
SS3	DL	Monotonic Test = 1.7 Cyclic Test 1 = 1.3 Cyclic Test 2 = 1.1 **Mean = 1.4**	Buckling of the diagonal braces in the out of plane direction Global rotation of the specimen due to different deformation of the braces	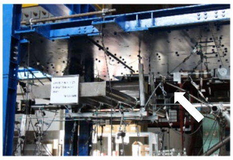
	LS	Monotonic Test = 17.0 Cyclic Test 1 = 13.6 Cyclic Test 2 = 12.3 **Mean = 14.3**	Significant deformation of the vertical and diagonal rods Rotation around the horizontal and perpendicular axis of the pipes The gravity load carrying capacity of the specimen was not compromised by the induced damage	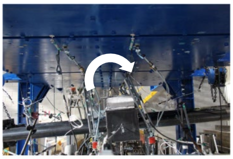 

- No brittle failure occurred in any of the tests. For the channel trapezes, the deformations were mainly concentrated in the components connecting the channel elements. For the rod trapezes significant deformations and buckling of the rods were observed.
- Independent of the failure mode and of the level of damage observed, no specimen lost its gravity load capacity in any test.
- All test specimens exhibited ductile behaviour. Higher ductility ratios were obtained for the rod trapezes (2.2 to 5.1) due to their lower yielding displacements compared to that of the channel configurations (1.5 to 3.8).
- Two performance objectives were identified for the performance-based seismic design of suspended piping restraint installations. The first damage limitation (DL) performance objective ensures that the functionality of the building is not affected and that the suspended piping restraints can be repaired economically. The second life-safety (LS) performance objective insures that the life-safety is not jeopardized and that the occupants can safely evacuate the building. This is achieved by ensuring that the suspended piping restraint installations are still able to carry the gravity loads (i.e. the weight of the pipes) safely.
- The tests showed also that the effective ductility factor (μ_{eff}), defined as the ratio of the ultimate to the yield displacements observed in each test, is an adequate and conservative EDP to predict the performance objectives described above. The DL performance objective is achieved for an effective ductility factor equal to unity, while the LS performance objective can be associated to the effective ductility factor (μ_{eff}) obtained from the tests at which the suspended piping restraint installations were still able to carry the gravity loads.

Table 9 Correlation between EDPs, onset of damage and performance objectives for configuration SS4

Configuration	Performance objective	EDP $\mu_{eff,exp}$	Damage description	Photographs
SS4	DL	Monotonic Test = 1.5 Cyclic Test 1 = 1.3 Cyclic Test 2 = 1.1 **Mean = 1.3**	Out of plane deformations of the diagonal rods Bending deformation of the horizontal channel as well as of the threaded rods connection the pipe rings to the horizontal channel	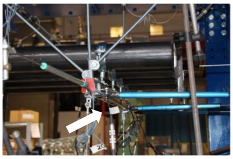
	LS	Monotonic Test = 3.5 Cyclic Test 1 = 6.7 Cyclic Test 2 = 7.4 **Mean = 5.9**	Significant rotation about the vertical axis of the specimen The vertical and diagonal threaded rods are significantly deformed. High torsional deformations of the horizontal channels near the connection with the vertical and diagonal rods The gravity load carrying capacity of the specimen was not compromised by the induced damage	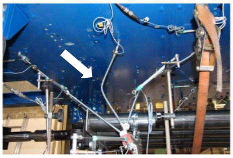 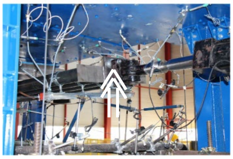

Acknowledgements The experimental study described in this paper was conducted as part of a collaborative research program between Hilti Corporation and the European Centre for Training and Research in Earthquake Engineering (EUCENTRE). The authors are grateful to Hilti Corporation for funding the experimental program. The technical staff of the ShakeLab Laboratory at EUCENTRE is also gratefully acknowledged for conducting the testing program described in this paper. The work has been also developed within the framework of the project "Dipartimenti di Eccellenza", funded by the Italian Ministry of University and Research (MUIR) at the University School for Advanced Studies IUSS Pavia.

References

ASCE (2016) ASCE 7-16: minimum design loads for buildings and other structures. American Society of Civil Engineers, Reston, p 889

CEN (2004) EN-1998-1:2004: Eurocode 8—design provisions for earthquake resistant structures. Comité Européen de Normalization, Brussels

Chock G, Robertson I, Nicholson P, Brandes H, Medley E, Okubo P, Hirshorn B, Sumada J, Kindred T, Linurna G, Sarwar A, Dal Pino J, Holmes W (2006) Compilation of observations of the October 15, 2006, Kiholo Bay (Mw 6.7) and Mahukona (Mw 6.0) earthquakes, Hawaii. Earthquake Engineering Research Institute, Oakland, p 53

FEMA (2003) Earthquake loss estimation methodology—HAZUS Technical Manual. Federal Emergency Management Agency, Washington, D.C.

FEMA (2007) FEMA 461: Interim testing protocols for determining the seismic performance characteristics of structural and nonstructural components. Federal Emergency Management Agency, Washington, D.C.

FEMA (2011) FEMA P-795: Quantification of building seismic performance factors: component equivalency methodology. Federal Emergency Management Agency, Washington, D.C.

FEMA (2012) FEMA E-74: Reducing the risks of nonstructural earthquake damage—a practical guide. Federal Emergency Management Agency, Washington, D.C.

FEMA (2018) FEMA P-58-1: Seismic performance assessment of buildings, vol 1. Federal Emergency Management Agency, Washington, D.C.

Filiatrault A, Sullivan T (2014) Performance-based seismic design of nonstructural building components: the next frontier of earthquake engineering. Earthq Eng Eng Vib 13(Suppl 1):17–46

Filiatrault A, Perrone D, Brunesi E, Beiter C, Piccinin R (2018) Effect of cyclic loading protocols on the experimental seismic performance evaluation of suspended piping restraint installations. Int J Pres Ves Pip 166:61–71

Fleming RP (1998) Analysis of fire sprinkler system performance in the Northridge Earthquake, Report No. NIST-GCR-98-636, U.S. Department of Commerce, Building and Fire Research Laboratory. National Institute of Standards and Technology, Gaithersburg, MD

Hilti (2014) Earthquake resistant design of installations, 1.1st edn. Schaan, Liechtenstein, p 104

Hoehler MS, Panagiotou M, Restrepo JI, Silva JF, Floriani L, Bourgund U, Gassner H (2009) Performance of suspended pipes and their anchorages during shake table testing of a seven-story building. Earthq Spectra 25(1):71–91

Jacobsen LS (1960) Damping in composite structures. Proc 2nd World Conf Earthq Eng 2:1029–1044

Kia M, Banazadeh M, Bayat M (2018) Rapid seismic vulnerability assessment by new regression-based demand and collapse models for steel moment frames. Earthq Struct 14(3):203–214

Kia M, Banazadeh M, Bayat M (2019) Rapid seismic loss assessment using new probabilistic demand and consequence models. B Earthq Eng 17(6):3545–3572

Krawinkler H (1999) Challenges and progress in performance-based earthquake engineering. International seminar on seismic engineering for tomorrow – in honor of professor Hiroshi Akiyama, Tokyo, Japan

Malhotra PK, Senseny PE, Braga AC, Allard RL (2003) Testing sprinkler-pipe seismic-brace components. Earthq Spectra 19(1):87–109

Miranda E, Taghavi S (2003) Estimation of seismic demands on acceleration-sensitive nonstructural components in critical facilities. In: Proceedings of the seminar on seismic design, performance, and retrofit of nonstructural components in critical facilities, ATC 29–2, Newport Beach, CA, pp 347–360

Miranda E, Mosqueda G, Retamales R, Pekcan G (2012) Performance of nonstructural components during the February 27, 2010 Chile Earthquake. Earthq Spectra 28(S1):S453–S471

NFPA (2019) NFPA 13: automatic sprinkler systems handbook. National Fire Protection Association Quincy, Massachusetts

O'Reilly GJ, Perrone D, Fox M, Monteiro R, Filiatrault A (2018) Seismic assessment and loss estimation of existing school buildings in Italy. Eng Struct 168(1):142–162

OSHPD (1995) The Northridge earthquake: a report to the hospital building safety board on the performance of hospitals. Office of Statewide Health Planning and Development, Facilities Development Division, Sacramento, California

Perrone D, Filiatrault A (2017) Automated seismic design of non-structural elements with building information modelling. Automat Constr 84:166–175

Perrone D, Calvi PM, Nascimbene R, Fischer E, Magliulo G (2018) Seismic performance and damage observation of non-structural elements during the 2016 Central Italy Earthquake. B Earthq Eng. https://doi.org/10.1007/s10518-018-0361-5

Sousa L, Monteiro R (2018) Seismic retrofit options for non-structural building partition walls: impact on loss estimation and cost-benefit analysis. Eng Struct 161:8–27

Tian Y, Filiatrault A, Mosqueda G (2014a) Experimental seismic fragility of pressurized fire suppression sprinkler piping joints. Earthq Spectra 30(4):1733–1748

Tian Y, Filiatrault A, Mosqueda G (2014b) Seismic response of pressurized fire sprinkler piping systems I: experimental study. J Earthq Eng 19(4):649–673

Wood RL, Hutchinson TC, Hoehler MS, Kreidl B (2014) Experimental characterization of trapeze assemblies supporting suspended non-structural systems. Proc. of the Tenth U.S. National Conference on Earthquake Engineering, Paper No. 905, Anchorage, Alaska, p 10

Yang TY, Moehle J, Stojadinovic B, Der Kiureghian A (2009) Seismic performance evaluation of facilities: methodology and implementation. J Struct Eng 135(10):1146–1154

Zaghi AE, Maragakis EM, Itani A, Goodwin E (2012) Experimental and analytical studies of hospital piping subassemblies subjected to seismic loading. Earthq Spectra 26(1):367–384

Publisher's Note Springer Nature remains neutral with regard to jurisdictional claims in published maps and institutional affiliations.